Termination-dependent edge states of MBE-grown WSe_{2}

Liwei Liu, Zhuozhi Ge, Chenhui Yan, Afsaneh Dorri Moghadam, Michael Weinert, and Lian Li

Phys. Rev. B **98**, 235304 — Published 28 December 2018

DOI: 10.1103/PhysRevB.98.235304

Termination-dependent edge states of MBE-grown WSe_2

Liwei Liu[†], Zhuozhi Ge[†], Chenhui Yan[†], Afsaneh Dorri Moghadam[‡], Michael Weinert[‡], Lian Li[*,†]

[†]Department of Physics and Astronomy, West Virginia University, Morgantown, WV, USA

[‡]Department of Physics, University of Wisconsin, Milwaukee, WI, USA

ABSTRACT

Using migration enhanced molecular beam epitaxy, we synthesize single- and bi-layer WSe_2 on epitaxial graphene/SiC(0001) and investigate the electronic properties of their edges with different terminations using scanning tunneling microscopy/spectroscopy (STM/S). Density functional theory calculations predict edge states at both Se and W edges, whose position and spatial distribution depend on how the edges are terminated. STS reveals that whether edge states at the nominal W edge are detectable depends on the number and spatial distribution of additional Se, whereas edge states on the Se edge are always detectable. Our findings indicate that edge termination plays an important role on edge states, and modification of the edge is a viable means to tailor the electronic properties of WSe_2 nanostructures.

*E-mail: lian.li@mail.wvu.edu

I. INTRODUCTION

Two-dimensional (2D) transition metal dichalcogenide (TMD) semiconductors have garnered tremendous interests in recent years due to their demonstrated remarkable properties and potential applications in nanoelectronics. Edges of 2D TMDs can play important roles in determining their electronic [1-5] and catalytic [6, 7] properties. For example: zigzag edges of MoS_2 nanoribbons are ferromagnetic and metallic, while armchair ones can be nonmagnetic and semiconducting [4]. Calculations [3, 8] and experiments [9-13] have also shown that edge morphology and termination can further modify the epitaxial growth of TMDs. For example, driven by the preferential formation of S-termination, size-dependence cluster morphology have been observed for MoS_2 nanostructures [13]. Thus, atomic scale studies of edge atomic and electronic properties are of great interest. As such, scanning tunneling microscopy/spectroscopy (STM/S) is ideally suited, as demonstrated by recent reports of edge states in bilayer (BL) WSe_2 [14].

Amongst the TMDs, monolayer WSe_2 is of particular interest owing to the observations of single photon emitters [15], as well as its large spin-orbit coupling [16, 17] that can enable novel valley-dependent phenomena and applications in spintronics and valleytronics [18-21]. While there has been investigations of edge states of BL WSe_2 by STM/S [14], the effects of different edge terminations are largely unknown. In addition, the TMDs films in these studies are mostly prepared by chemical vapor deposition and transferred in air to ultrahigh vacuum system for STM/S investigations. As the TMD edges are particularly prone to oxidation [22-24], this air exposure can significantly compromise the investigation of the intrinsic properties of the edges. In fact, even metallic WSe_2 edges have been observed due to air exposure [25].

Here we synthesize mono- and bi-layer WSe_2 on epitaxial graphene (EG)/SiC(0001) substrates via migration enhanced molecular beam epitaxy (MBE) [9, 26], and investigate their edge states by *in situ* scanning tunneling microscopy/spectroscopy and density functional theory (DFT) calculations. By carrying out MBE growth, sample transfer, and measurements strictly under UHV conditions, any contamination that may occur in ambient environments is minimized, allowing the investigation of intrinsic properties of WSe_2 edges. Three types of edges were investigated: Se edges, and W edges saturated by either one or two Se atoms per W atom (denoted as W_{Se} and W_{2Se} edge, respectively). We observe edge states for both the Se and W_{2Se} as predicted by DFT calculations, however on W_{Se} edges, the predicted edge states are not detected by STS: this apparent discrepancy is due to the small contribution of these particular edge states to the local density of states (LDOS) in the vacuum region probed in STS, an effect that is captured in our STS simulations.

II. EXPERIMENTAL AND COMPUTATIONAL METHOD

Experimental method: Molecular beam epitaxy (MBE) and STM experiments were performed in an interconnected ultrahigh vacuum (UHV) system (base pressure 1×10^{-10} mbar) comprising of MBE chambers and two Omicron STMs (a variable-temperature and the other low-temperature (6 K)), while the XPS and Raman spectroscopy were performed *ex-situ*. Epitaxial graphene (EG) was grown by thermal decomposition of 6H-SiC(0001) [27], which was first prepared by removal of polishing damages in a H_2/Ar atmosphere between 1500 and 1600 ℃. After degassing in UHV, the SiC sample was heated to 1100~1300 ℃ for 15 min for the growth of graphene.

WSe_2 films were prepared by migration enhanced MBE [26] with a deposition rate of ~0.5 ML/hr. W was provided using a QUAD e-beam evaporators (Mantis Deposition Ltd), while the

elemental Se source in a Knudsen cell heated to 120 ℃. The ratio of W to Se is about 1:60. During film deposition, the background pressure in the chamber was ~5.0 × 10^{-9} mbar. The EG/SiC substrate was kept at 350~500℃ during deposition and post-annealed at the same temperature for an hour to desorb excess Se.

STM imaging was carried out with electrochemically etched W tips at room temperature and liquid nitrogen temperature in UHV. The dI/dV tunneling spectra were acquired using lock-in detection at liquid nitrogen temperature by applying an AC modulation of 20 mV (r.m.s.) at 860 Hz to the bias voltage. Each single spectrum shown in the manuscript was the average of 10 spectra.

DFT calculations: The monolayer-bilayer system was modeled by a ribbon of 16 unit cells (~4.4 nm) on a continuous 24 unit cell layer, with ~2.4 nm separation between ribbons. The electronic structure was calculated using VASP, including both spin-polarization and spin-orbit, with the PBE functional and D3 van der Waals corrections, and wave function cutoff of 400 eV. While the local band structures are determined in the standard manner of integrating the wave functions over local boxes that include the atomic cores, the simulation of the STS spectra – which are related to the local density of states (LDOS) at the position of the tip – proceeds differently. To include varying height of the tip above the surface varies, the LDOS were calculated along an isosurface (and integrated perpendicular to the plots) corresponding to using the -2 V bias used in the constant current experiment. This procedure thus can account for variations in the STS spectra with bias and current set points (which determine the height of the tip) and for the spatial distribution of the states. The Se sites on the Se edge of the ribbons have calculated moments of ~0.2 μ_B/Se. On the W-terminated edges, the total moments are 1.43 for ideal the W edge, 1.08 μ_B for the W_{Se} edge, and 1.27 μ_B for the W_{2Se} edge.

III. RESULTS AND DISCUSSION

Shown in Fig. 1 is the WSe_2 film morphology as a function of growth conditions such as substrate temperature and W/Se flux ratio (typically very Se-rich conditions, e.g., W/Se~1:60). At low substrate temperatures (e.g., 350 ^oC) and relatively high growth rate (e.g., 2ML/hr), the WSe_2 islands nucleate in fractal shapes without any three-fold symmetry [Fig. 1(a)]. At 500 ^oC, the growth transitions from fractal to compact, and begins to exhibit some three-fold symmetry [Fig. 1(b)]. However, further increasing the substrate temperature leads to substantial desorption of Se. To mitigate this effect, we employ migration-enhanced MBE, where the Se flux is kept constant, while the W flux is reduced by switching the W shutter on and off periodically (e.g., W shutter on for 1 minute and off for 3 minutes). This process enhances the migration of the W adatoms on the surface and hence diffusion length, before incorporating at more favorable sites, i.e., edges of existing 2D islands. Using this method, we have grown compact triangular islands with island edges up to 80 nm [Fig. 1(c)]. *Ex situ* XPS and Raman measurements of the WSe_2 films confirm that they are the 2H polytype of the WSe_2 [See Supplemental Material Fig. S1 [28]].

Close-up view of the SL WSe_2 reveals a (3 × 3) Moiré pattern, consistent with the lattice mismatch between WSe_2 and EG (lattice constants of 0.33 and 0.25 nm, respectively) [Fig. 1(d)]. This periodicity also indicates that the SL WSe_2 and the underlying EG are rotationally aligned. Thus, as indicated by the arrows in Fig. 1(c), most of the edges of the triangular islands are along the atomic lattice of WSe_2, i.e., terminated with zigzag rather than armchair edges. This is consistent with previous work that have shown zigzag edges to be the energetically favorable edges [14, 29, 30].

The electronic properties of SL and BL WSe_2 are investigated by dI/dV tunneling spectroscopy, as shown in Fig. 2. With feedback OFF [Fig. 2(b)], the dI/dV spectrum for SL WSe_2 exhibits a prominent peak at -1.5 V with a gradual onset at -1.25 eV. Since the onsets in the dI/dV spectra typically correspond to valence band maximum (VBM) and conduction band minimum (CBM) edges, this gives rise to an "apparent" VBM and CBM at -1.25 and 1.1 eV, respectively. For the BL WSe_2 [Fig. 1(c)], the dI/dV spectrum exhibits two peaks at -1.0 and -1.7 eV, with an apparent VBM and CBM at -0.75 and 1.1 eV, respectively. Note that the dI/dV conductance in both cases is close to zero within the band gap, indicating that the contributions from the EG/SiC substrate are negligible in this region. This further confirms that the intrinsic properties of WSe_2 are preserved on the EG/SiC substrates, in contrast to that on metal substrates such as Au(111) where background conductance is also measured [2, 31].

Since it is challenging to resolve the exact onset energy positions of semiconductor band edges with the feedback OFF, dI/dV spectra were also recorded with feedback ON [16], as shown in Fig. 2(d). For SL, two peaks are apparent, a small one at -1.10 eV and a large peak at -1.57 eV, attributed to states at K and Γ, respectively, based on comparison to DFT calculated bands as shown in Fig. 2(e). Within the standard model for STM [32, 33], states at K have much faster decay than those at Γ due to the parallel momentum contribution to the decay of the wave function in the vacuum. Thus in dI/dV with feedback OFF [Fig. 2(b)], only a prominent peak at -1.5 eV is seen from states at Γ. Similarly for BL, two peaks at -0.89 and -1.69 eV are observed with feedback ON, corresponding to that seen with feedback OFF [Fig. 2(c)]. Comparison with the calculated bands [Fig. 2(f)] attribute these peaks to states from Γ_1 and Γ_2, with the latter at higher energy. From the peak separation in Figs. 2(b) and 2(c), it can be determined that the K-Γ

splitting is $\Delta_{K-\Gamma} = 0.49 \pm 0.06$ eV for SL, and Γ-Γ splitting is $\Delta_{\Gamma-\Gamma} = 0.79 \pm 0.12$ eV for BL, both of which are consistent with previous work [14, 17].

Based on these results, an improved estimation of the band gap is obtained by subtracting the K-Γ splitting from the apparent gap, yielding 2.26 ± 0.05 eV for SL and 1.94 ± 0.08 eV for BL. Note, our DFT calculations indicate that both SL and BL WSe_2 are indirect gap semiconductors [Figs. 2(e) and 2(f)], consistent with the experimental dZ/dV observation [16], in contrast to MoS_2 and $MoSe_2$ [34] where SLs exhibit a direct gap.

Next, to gain insights into the influence of edge terminations on the edge states, we calculate the electronic properties of BL $WeSe_2$ edges. To simplify the calculation, we ignore graphene and model the SL-BL system as SL zigzag WSe_2 ribbons supported on an infinite SL WSe_2 [See Supplemental Material Fig. S2 [28]]. At the center of the supported ribbon (BL region), the electronic structure, particularly the size of the band gap and the band extrema, are essentially the same as in infinite BL, and similarly for the SL regions [Figs S2(c) and S2(d) [28]]. At the edges of BL zigzag ribbon, one edge is normally Se terminated, while the opposite is W terminated. The breaking of W-Se network naturally leads to edge states due to dangling bonds.

To simulate the Se-rich growth conditions, the W atoms at the edges are saturated with extra Se atoms. Three configurations with different numbers of Se atoms were considered [Figs. 3(a-c)]: while all Se edges are terminated with two Se atoms per W atom; the opposite W edge is saturated with 0, 1, or 2 Se atoms per W, denoted as W, W_{Se}, and W_{2Se} edge, respectively. As shown in Figs. 3(d-f), at the Se edge (left panels), there are two sets of edge states: one set of exchange-split states coming off the valence band and another splitting off the conduction band extending to mid-gap. These states are observable by dI/dV tunneling spectroscopy as discussed in more details below.

For the bare W edge termination, there are a large number of edge states within the gap [Fig. 3(d)]. For the W_{Se} edge, the edge states are reduced. There are again two sets of edge state bands pulled off the top of the BL valence bands, and another set dispersing upward from mid-gap into the conduction bands [Fig. 3(e)]. However, the STS-simulated LDOS at the W_{Se} edge is small. This difference stems from the fact that the bands in Figs. 3(d-f) are weighted by their wave function contribution throughout the whole thickness of the ribbon, while the LDOS is evaluated at the position of the tip above the surface determined by the bias voltage. Thus, edge states that do not project into the vacuum region (e.g., p_x/p_y states of the Se on the W_{Se} edge) will have only small contributions to the LDOS and STS, i.e., the plotted bands and LDOS are sampling different regions of space, both of which are needed to interpret the experimental results. Similar orbital spatial distribution effect has been reported at W vacancies in SL WSe_2 films, where calculations showed significant in-gap states at the W vacancy that were not observed in STS [35]. On the other hand, for the W edge saturated by two Se atoms, the extra Se atom has orbital contributions extending further into the vacuum region, and is readily observable by STS, as discussed below.

For the hexagonal and/or truncated triangular WSe_2 islands, the two opposite parallel edges, or edges with an angle of 120^o between them, are A and B edges with different terminations [Fig. 4(a)]. As seen in Fig. 4(b), at the center of the island, the prominent feature at -1.5 and -0.75 eV correspond to the onset of states arising from Γ_1 and Γ_2, respectively [Fig. 2(c)]. At the left edge of the island (point 3), edge states emerge from -0.46 eV and merges with the bulk VB up to -2.0 eV. The CB onset is at 0.99 eV, slightly lower than the bulk value at 1.13 eV. At this edge, since it is difficult to distinguish edge states from the bulk gap, we report a value of "apparent band gap" instead, as defined by the separation between onsets of the occupied and unoccupied states,

i.e., 1.45 eV at point 3. Note that the edge states spatially extend from point 2 to 4, and comparison with the calculated bands in Fig. 3 suggest that this is the Se terminated edge.

At the right edge of the island (point 13), no signature of edge states is found. The VB and CB band edges are -1.28 and 1.15 eV, respectively, yielding an "apparent band gap" of 2.43 eV in this case, greater than that at the center of the BL island. This feature is consistent with the W + 1 Se case in the calculations [Fig. 3(e)], where the LDOS (x) of W_{Se} edge shows a downward shift of the edge of the occupied states, as well as states pulled down from the bottom of the conduction band. From the calculations for the W+1 Se case, the Se edge and W_{Se} edge have local gaps of 1.4 and 2.3 eV, in agreement with our experimental observations of 1.45 and 2.43 eV. Comparison of these experimental and theoretical results leads to the assignment that edge A is the Se terminated, and edge B is a W_{Se} edge.

While the majority of the islands show this distinct difference for the "apparent band gap" of the two types of edges, with the edge states detectable at only one type of edge, WSe_2 islands where both type A and B edges (adjacent edges rotated by 120^o) show in-gap edge states exist, as shown in Fig. 5(a). Although the spectra may be expected to be similar to that in Fig. 4, from Figs. 5(b)-(d), it is seen that both edges show pronounced edge states with very similar features: both exhibit peaks at -1.0 and -1.5 eV and rise further to -2.0 eV, and at CB, both rise at ~1.0 eV. The apparent gaps are 1.5 and 1.3 eV for the Se and W edge, respectively. Comparison to calculated bands in Fig. 3 suggests a W edge terminated with two Se atom (2 Se/W). Calculations in Fig. 3(c) indicate that both edges exhibit edge states, with apparent gaps of 1.4 and 1.2 eV, consistent with our experimental observations. Intuitively, the W_{2Se} edges have similar orbital spatial distribution to the Se edge, and this structural similarity gives rise to the similar electronic structures at these edges. Overall our findings indicate that edge states are

highly dependent on the termination and orbital spatial distribution of the atoms at the edges, and can significantly alter the bandgap by as much as 1 eV. It further suggests that the electronic properties of WSe_2 nanostructures can be tailored by engineering edge terminations. The presence of these edge states can also be expected to affect lateral and vertical transport, and should be taken into account when designing heterostructures and contacts for device applications.

VI. CONCLUSIONS

In conclusion, we have synthesized single and bilayer WSe_2 on EG/SiC(0001) by migration enhanced MBE. Our findings indicate that while there are always edge states at the Se edge originating from the valence bands, the observation of edge state at W edges depends on the numbers of Se atoms attached to the W atoms. For the 1 Se/W termination case, the contribution of the edge state to the LDOS is weak due to the spatial distribution of the wave function. In contrast, edge states are pronounced for the 2 Se/W case. Comparison between our experimental observation and DFT calculations suggests that our WSe_2 edges are primarily terminated with 1 Se atoms per W. Our results provide new insights into the impact of edge terminations on edge states in WSe_2, critical for designing future TMD-material-based electronic devices and may also be applicable to other 2D TMD materials.

ACKNOWLEDGMENTS

We acknowledge funding by the NSF (DMR-1734017).

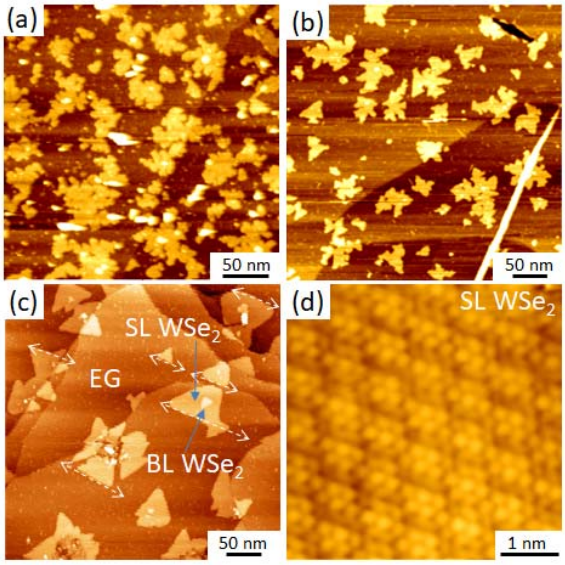

Fig. 1

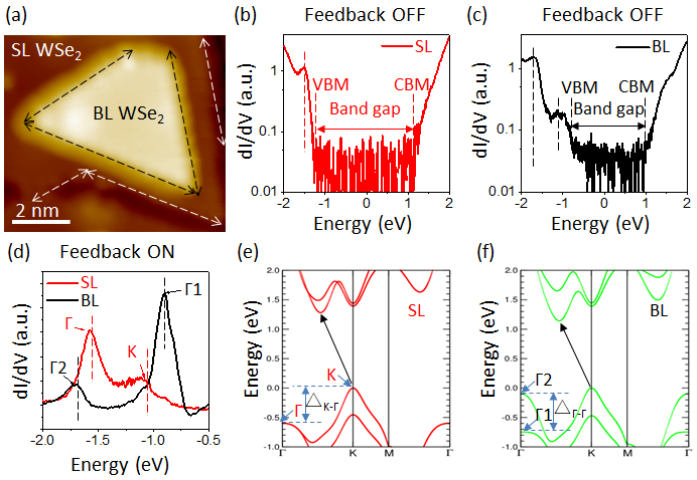
(a)
SL WSe2
BL WSe2
2 nm
(b)
Feedback OFF
SL
VBM
CBM
Band gap
dI/dV (a.u.)
Energy (eV)
(c)
Feedback OFF
BL
VBM
CBM
Band gap
dI/dV (a.u.)
Energy (eV)
(d)
Feedback ON
SL
BL
Γ
Γ1
Γ2
K
dI/dV (a.u.)
Energy (eV)
(e)
SL
K
Γ
K-Γ
Energy (eV)
Γ
K
M
Γ
(f)
BL
Γ2
Γ1
Γ-Γ
Energy (eV)
Γ
K
M
Γ

Fig. 2

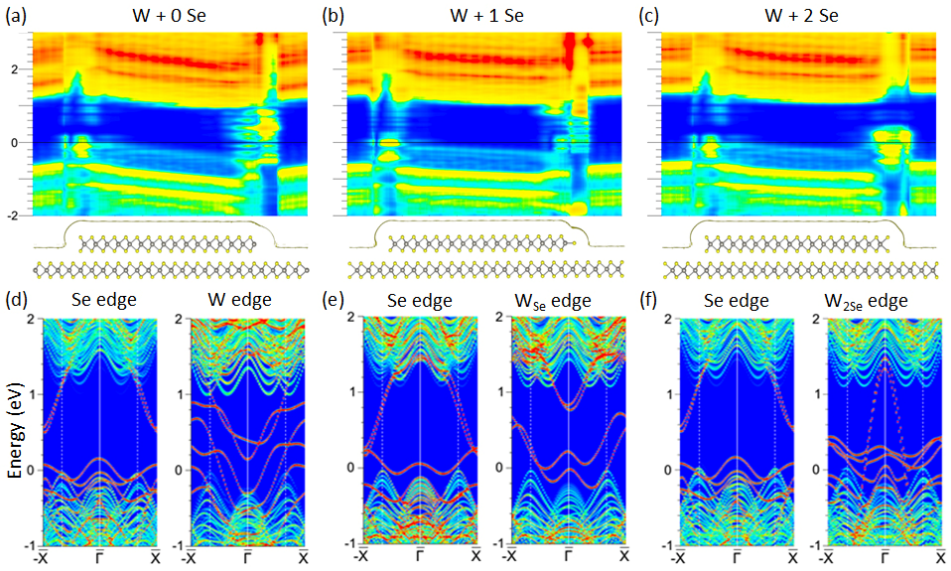
(a)
W + 0 Se
(b)
W + 1 Se
(c)
W + 2 Se
(d)
Se edge
W edge
(e)
Se edge
W_{Se} edge
(f)
Se edge
W_{2Se} edge
Energy (eV)
2
1
0
-1
-X̄
Γ̄
X̄

Fig. 3

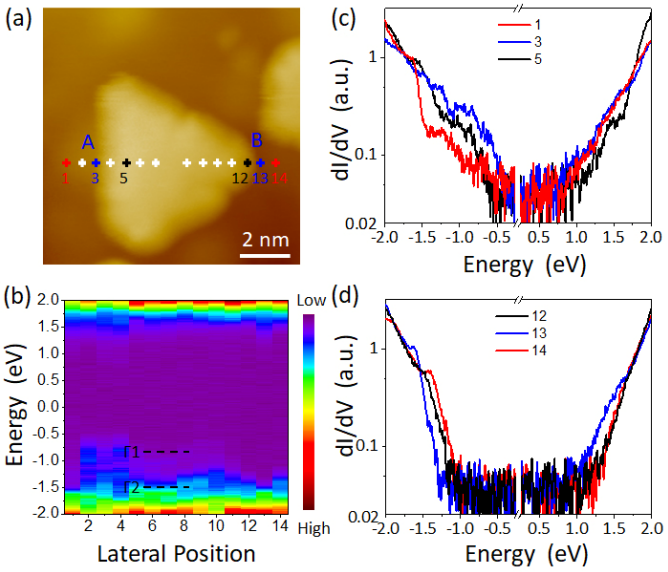
(a)
A
B
1
3
5
12
13
14
2 nm
(c)
1
3
5
dI/dV (a.u.)
Energy (eV)
(b)
Energy (eV)
Lateral Position
Low
High
Γ1
Γ2
(d)
12
13
14
dI/dV (a.u.)
Energy (eV)

Fig. 4

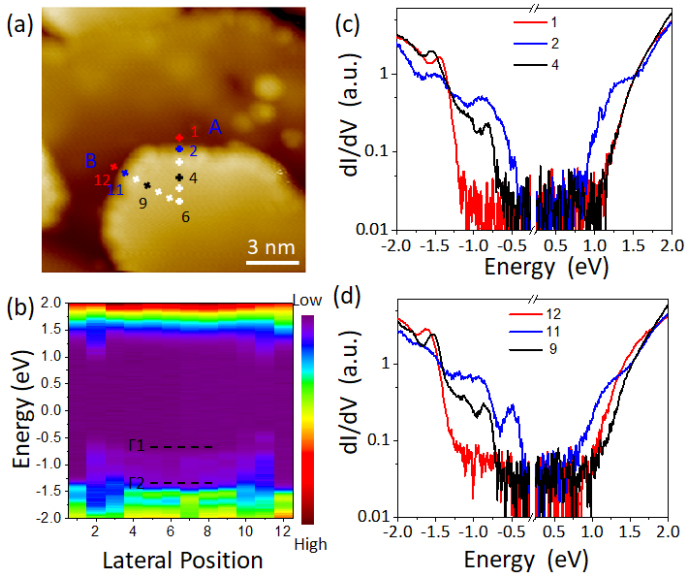
(a)
A
B
1
2
4
6
9
11
12
3 nm
(b)
Energy (eV)
Lateral Position
Low
High
F1
F2
(c)
dI/dV (a.u.)
Energy (eV)
1
2
4
(d)
dI/dV (a.u.)
Energy (eV)
12
11
9

Fig. 5

Figure captions:

Fig. 1. STM images of MBE-grown WSe_2 on EG/SiC: (a) low substrate temperature (350 ^oC) and high growth rate (2 ML/hr), (b) high substrate temperature (500 ^oC) and high growth rate (2 ML/hr), (c) high substrate temperature (500 ^oC) and low growth rate (0.5 ML/hr) with migration enhanced MBE. (d) Close up view of SL WSe_2/EG, showing the (3x3) Moiré pattern. Imaging parameters: (a) 300 × 300 nm, V_s =3.2 V, I_t =0.1 nA; (b) 400 × 400 nm, V_s =3.3 V, I_t =0.16 nA; (c) 390 × 390 nm, V_s =1.96 V, I_t =0.15 nA; (d) 6 × 6 nm, Vs=0.1 V, I_t=0.1 nA.

Fig. 2. (a) The STM image of SL and BL WSe_2 on epitaxial graphene. (b-d) dI/dV spectra measured at the center of SL and BL WSe_2 with feedback OFF (b and c) and ON (d), respectively. (e) and (f) Calculated band structure of SL and BL WSe_2, respectively. Imaging parameters: (a) 42 × 42 nm, V_s= -2 V, I_t=0.01 nA; STS settings before opening feedback loop: -2 V, 20 pA.

Fig. 3. Calculated LDOS and local electronic bands for BL WSe_2 island (SL WSe_2 ribbons on SL WSe_2), for different terminations of the W edge of the ribbon: (a),(d) W termination with 0 Se attachment per W atom (Se/W), (b),(e) W termination with 1 Se/W. (c),(f) W termination with 2 Se/W. Schematics of the structures and the surface used for the calculation of the LDOS are shown in the middle row. The white dotted lines indicate the position where the bulk K, K' points will project for the zigzag ribbons. Note that the edge states for *k* and -*k* differ as a result of the breaking of time-reversal (magnetic edges) and spin-orbit.

Fig. 4. (a) STM image of a SL WSe_2 island on top of SL WSe_2 film. (b) Real space plot of the band profile, taken along the positions labeled in (a). (c) and (d) dI/dV spectra at the *A* and *B* edges of the BL WSe_2 island. The blue curves are taken at the edge, while the red and black curves are taken at the adjacent points at SL and BL, respectively. Imaging parameters: (a) 10 × 12 nm, V_s = -2 V, I_t =0.1 nA. STS settings before opening feedback loop: -2 V, 20 pA.

Fig. 5. (a) STM image of a SL WSe_2 island on top of SL WSe_2. (b) Real space plot of the band profile, taken along the positions labeled in (a). (c) dI/dV taken at the *A* edge of the WSe_2 junction. The blue curves are taken at edges, while the red and black curves are taken at the adjacent points at SL and BL, respectively. (d) dI/dV at the edges of the *B* edge of the WSe_2 junction. The blue curves are taken at edges, while the red and black curves are taken at the adjacent points at SL and BL, respectively. Imaging parameters: (a) 15 × 15 nm, V_s =2.0 V, I_t =0.1 nA. STS settings before opening feedback loop: -2 V, 20 pA.

REFERENCES

[1] R.-L. Chu, G.-B. Liu, W. Yao, X. Xu, D. Xiao, and C. Zhang, Phys. Rev. B **89**, 155317 (2014).
[2] M. V. Bollinger, J. V. Lauritsen, K. W. Jacobsen, J. K. Norskov, S. Helveg, and F. Besenbacher, Phys. Rev. Lett. **87**, 196803 (2001).
[3] D. Cao, T. Shen, P. Liang, X. Chen, and H. Shu, J. Phys. Chem. C **119**, 4294 (2015).
[4] Y. Li, Z. Zhou, S. Zhang, and Z. Chen, J. Am. Chem. Soc. **130**, 16739 (2008).
[5] G. Xu, J. Wang, B. Yan, and X.-L. Qi, Phys. Rev. B **90**, 100505 (2014).
[6] T. F. Jaramillo, K. P. Jørgensen, J. Bonde, J. H. Nielsen, S. Horch, and I. Chorkendorff, Science **317**, 100 (2007).
[7] C. Tsai, K. Chan, F. Abild-Pedersen, and J. K. Norskov, Phys. Chem. Chem. Phys. **16**, 13156 (2014).
[8] Y. Nie, C. Liang, K. Zhang, R. Zhao, S. M. Eichfeld, P.-R. Cha, L. Colombo, J. A. Robinson, R. M. Wallace, and K. Cho, 2D Mater. **3**, 025029 (2016).
[9] R. Yue, Y. Nie, L. A. Walsh, R. Addou, C. Liang, N. Lu, A. T. Barton, H. Zhu, Z. Che, D. Barrera *et al.*, 2D Mater. **4**, 045019 (2017).
[10] L. Jiao, H. J. Liu, J. L. Chen, Y. Yi, W. G. Chen, Y. Cai, J. N. Wang, X. Q. Dai, N. Wang, W. K. Ho *et al.*, New J. Phys. **17**, 053023 (2015).
[11] S. Vishwanath, A. Sundar, X. Liu, A. Azcatl, E. Lochocki, A. R. Woll, S. Rouvimov, W. S. Hwang, N. Lu, X. Peng *et al.*, J. Cryst. Growth **482**, 61 (2018).
[12] D. Y. Fu, X. X. Zhao, Y. Y. Zhang, L. J. Li, H. Xu, A. R. Jang, S. I. Yoon, P. Song, S. M. Poh, T. H. Ren *et al.*, J. Am. Chem. Soc. **139**, 9392 (2017).
[13] J. V. Lauritsen, J. Kibsgaard, S. Helveg, H. Topsoe, B. S. Clausen, E. Laegsgaard, and F. Besenbacher, Nat. Nanotechnol. **2**, 53 (2007).
[14] C. Zhang, Y. Chen, J. K. Huang, X. Wu, L. J. Li, W. Yao, J. Tersoff, and C. K. Shih, Nat. Commun. **6**, 10349 (2016).
[15] M. Koperski, K. Nogajewski, A. Arora, V. Cherkez, P. Mallet, J. Y. Veuillen, J. Marcus, P. Kossacki, and M. Potemski, Nat. Nanotechnol. **10**, 503 (2015).
[16] C. Zhang, Y. Chen, A. Johnson, M. Y. Li, L. J. Li, P. C. Mende, R. M. Feenstra, and C. K. Shih, Nano Lett. **15**, 6494 (2015).
[17] Y. Zhang, M. M. Ugeda, C. H. Jin, S. F. Shi, A. J. Bradley, A. Martin-Recio, H. Ryu, J. Kim, S. J. Tang, Y. Kim *et al.*, Nano Lett. **16**, 2485 (2016).
[18] X. Xu, W. Yao, D. Xiao, and T. F. Heinz, Nat. Phys. **10**, 343 (2014).
[19] G. Aivazian, Z. Gong, A. M. Jones, R.-L. Chu, J. Yan, D. G. Mandrus, C. Zhang, D. Cobden, W. Yao, and X. Xu, Nat. Phys. **11**, 148 (2015).
[20] K. Hao, G. Moody, F. Wu, C. K. Dass, L. Xu, C.-H. Chen, L. Sun, M.-Y. Li, L.-J. Li, A. H. MacDonald *et al.*, Nat. Phys. **12**, 677 (2016).
[21] A. M. Jones, H. Yu, J. S. Ross, P. Klement, N. J. Ghimire, J. Yan, D. G. Mandrus, W. Yao, and X. Xu, Nat. Phys. **10**, 130 (2014).
[22] J. H. Park, S. Vishwanath, X. Liu, H. Zhou, S. M. Eichfeld, S. K. Fullerton-Shirey, J. A. Robinson, R. M. Feenstra, J. Furdyna, D. Jena *et al.*, ACS Nano **10**, 4258 (2016).
[23] J. H. Park, S. Vishwanath, S. Wolf, K. Zhang, I. Kwak, M. Edmonds, M. Breeden, X. Liu, M. Dobrowolska, J. Furdyna *et al.*, ACS Appl Mater Interfaces **9**, 29255 (2017).
[24] R. C. Longo, R. Addou, S. Kc, J.-Y. Noh, C. M. Smyth, D. Barrera, C. Zhang, J. W. P. Hsu, R. M. Wallace, and K. Cho, 2D Mater. **4**, 025050 (2017).

[25] R. Addou, C. M. Smyth, J. Y. Noh, Y. C. Lin, Y. Pan, S. M. Eichfeld, S. Folsch, J. A. Robinson, K. Cho, R. M. Feenstra *et al.*, 2d Materials **5**, 2018).
[26] L. A. Walsh, R. Yue, Q. Wang, A. T. Barton, R. Addou, C. M. Smyth, H. Zhu, J. Kim, L. Colombo, M. J. Kim *et al.*, 2D Mater. **4**, 025044 (2017).
[27] Y. Y. Li, M. X. Chen, M. Weinert, and L. Li, Nat. Commun. **5**, 4311 (2014).
[28]See Supplemental Material at [URL] for XPS, Raman measurements and additional details on DFT calculations.
[29] D. Davelou, G. Kopidakis, E. Kaxiras, and I. N. Remediakis, Phys. Rev. B **96**, 165436 (2017).
[30] Y. Chen, P. Cui, X. Ren, C. Zhang, C. Jin, Z. Zhang, and C. K. Shih, Nat. Commun. **8**, 15135 (2017).
[31] J. Lu, D. L. Bao, K. Qian, S. Zhang, H. Chen, X. Lin, S. X. Du, and H. J. Gao, ACS Nano **11**, 1689 (2017).
[32] J. Tersoff, and D. R. Hamann, Phys. Rev. Lett. **50**, 1998 (1983).
[33] J. Tersoff, and D. R. Hamann, Phys. Rev. B **31**, 805 (1985).
[34] Y. Zhang, T. R. Chang, B. Zhou, Y. T. Cui, H. Yan, Z. Liu, F. Schmitt, J. Lee, R. Moore, Y. Chen *et al.*, Nat. Nanotechnol. **9**, 111 (2014).
[35] S. Zhang, C. G. Wang, M. Y. Li, D. Huang, L. J. Li, W. Ji, and S. Wu, Phys. Rev. Lett. **119**, 046101 (2017).